Macromolecules **1985**, *18*, 2208–2215

Restricted Rotational Diffusion of a Rodlike Solvent in a Polymeric Matrix

Nelson H. Oliver and R. Pecora*

Department of Chemistry, Stanford University, Stanford, California 94305

A. C. Ouano

IBM Corporation, San Jose, California 95193. *Received November 19, 1984*

ABSTRACT: Fabry–Perot interferometry is used to observe the depolarized dynamic light scattering (DDLS) spectra of *p*-chlorodiphenylmethane (CPM) and of poly(methyl methacrylate) mixtures with CPM. The DDLS spectra are recorded from −4 to +98 °C with several experimental interferometer spacings, which allow detection of reorientational motion throughout the 20-MHz to 100-GHz range. Rotational diffusion of CPM consistent with hydrodynamics is the sole reorientational relaxation mechanism seen in the neat liquid above −4 °C, but the polymer-containing samples also relax on slower time scales. Sound speeds in all the samples and the viscosity, density, and refractive index of neat CPM are also reported. The DDLS spectral features of the polymer-containing samples are interpreted with the restricted rotational diffusion (RRD) theory of Wang and Pecora and found to be in qualitative agreement. The quantitative discrepancy between the theory and experiment is attributable to the relaxation of the hindering environment, which is not included in the simple RRD model.

Introduction

The use of dynamic light scattering (DLS) to study amorphous media is now common.[1-3] In this paper we extend the work of Ouano and Pecora[4] on rotational motion of small rodlike probes in a poly(methyl methacrylate) (PMMA) matrix. For a general comprehensive discussion of theory and applications of DLS, the interested reader is referred to the book of Berne and Pecora.[5]

Molecular motion in amorphous samples is not only important because of the increasing prevalence of plastics and other new technologies, such as amorphous semiconductors; the fluid states are inherently intriguing because of their complexity. It is hoped that observation of a wide variety of amorphous fluids will reveal the common elements of their dynamics and lead to general models for their behavior.

In this experiment, five PMMA samples plasticized with 20–58% (w/w) *p*-chlorodiphenylmethane (CPM) are studied by Fabry–Perot interferometry in the temperature range −4.5 to +98 °C. Since CPM has nearly the same refractive index as PMMA, the light scattering from concentration fluctuations is minimal. The depolarized light scattering may then be clearly observed and interpreted as rotational relaxation of CPM. The rotational diffusion coefficients from CPM/PMMA samples are compared to the rotational rates and shear viscosities of neat CPM. The results are interpreted with the restricted rotational diffusion (RRD) model of Wang and Pecora,[6] which is also known as the "diffusion-in-a-cone" model. The concentration dependence of the rotational rates is fit with the semiempirical expressions for viscosity developed by Doolittle.[7]

Experimental Section

A complete discussion of the preparation of optical-quality PMMA samples is given by Ouano and Pecora.[4] The important features of the procedure follow.

The optical measure of purity in polymeric samples is the Landau–Placzek ratio: the intensity of the unshifted spectral component divided by the intensity of the Brillouin satellites. Values as low as 4 have been reported for bulk PMMA, though a more typical value is 10. The PMMA used here is made by free radical initiated thermal polymerization, giving an atactic product. Plasticizing bulk PMMA with a good solvent like CPM softens the matrix, allowing some of the strain to be relaxed. The solvent also fills voids in the polymer matrix, minimizing light scattering by refractive index fluctuations. Because these samples are studied near their glass transition temperatures (T_g), they must be annealed at no more than 10 °C/day to minimize thermal strain-induced light scattering.

Therefore, thermal polymerization of scrupulously pure reactants and subsequent slow annealing from the 115 °C reaction temperature can give CPM/PMMA samples near their T_g of high optical quality. Experimental Landau–Placzek ratios for the samples studied here range from 3 for 58% CPM at 98 °C to ~100 for 20% CPM at −4.5 °C. The 20% CPM sample has typically 3 times the Landau–Placzek ratio of the 58% CPM sample at the same temperature because of the greater strain in the more immobile 20% CPM sample. Higher values of the ratio at low temperature are due to residual strain from annealing at a finite rate and are fully reversible with return to higher temperatures. It must be emphasized that the Landau–Placzek ratios measured here are not directly comparable with those reported for bulk PMMA, since the polarized scattered intensity is due to the solvent as well as the polymer. However, the temperature dependence of the observed Landau–Placzek ratios for the CPM/PMMA samples is a useful measure of their general purity and thermal strain-induced light scattering intensity.

Viscosity and depolarized light scattering studies were also performed for neat liquid CPM. Fabry–Perot spectra of neat CPM are collected over the entire −4.5 to +98 °C experimental range, giving the rotational diffusion coefficient and its temperature dependence for the rotation of CPM unhindered by PMMA. The kinematic viscosity of neat CPM and its temperature dependence are then obtained with a 3-cm^3 capillary viscometer immersed in an alcohol/water constant-temperature bath. The CPM is then transferred to a custom-made 1.5-cm^3 micropycnometer to record its density as a function of temperature. Both the viscometer and micropycnometer are standarized prior to use with methanol and carbon tetrachloride at 0–36 °C against the literature values.[8]

The dynamic light scattering apparatus consists of a Spectra Physics 165 Ar^+ laser that is etalon-locked in the light control mode at 488-nm wavelength to produce 600 mW of continuous TEM_{00} radiation that illuminates the cylindrical quartz cell in which the sample is prepared. The light scattered by the sample at 90° is collected through a Glan–Thompson polarizer whose extinction coefficient is 10^{-6} and into a piezoelectrically scanned Fabry–Perot interferometer, which may be equipped with spherical mirrors for a 750-MHz free spectral range (FSR) or flat plates for an adjustable FSR up to ~100 GHz. The light transmitted by the interferometer impinges on an EMI photomultiplier, whose output is digitized with an SSR 1105 photon counter and then is analyzed with a Nova 3 computer.

The incident light beam is vertically plane-polarized normal to the scattering plane defined by the incident and collected beams (Figure 1). A polarizer transmits only the horizontally polarized component of the collected beam, lying in the scattering plane. With this arrangement, only those scattering processes that rotate

0024-9297/85/2218-2208$01.50/0

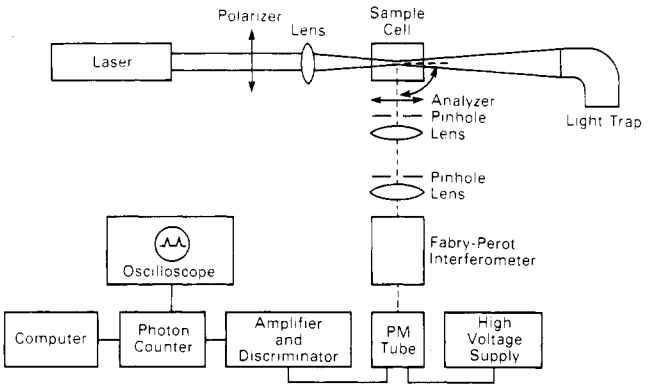

Figure 1. Dynamic light scattering experiment. Schematic of a typical Fabry–Perot frequency-scanning instrument as used in this study.

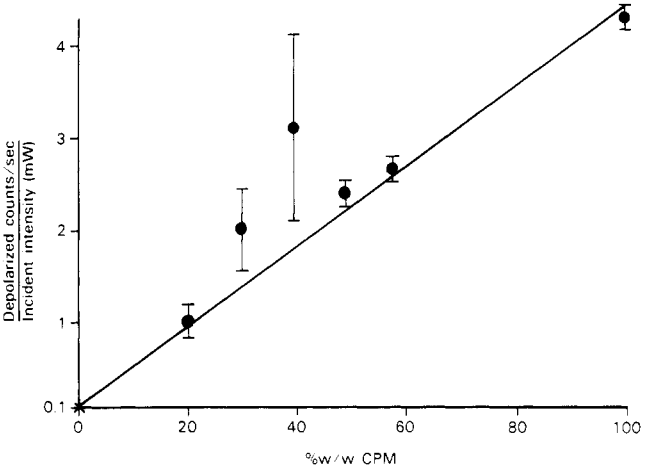

Figure 2. Normalized depolarized scattering intensity is linear in CPM concentration for the undamaged samples.

the plane of polarization contribute intensity at the detector. This VH or depolarized component is due mainly to molecular optical anisotropy and to fluorescence. In the spectral range accessible to this experiment, fluorescence appears as an increase in the base line of the depolarized DLS (DDLS) spectrum, which may be removed with a 488-nm spike filter in the collection optics. In these experiments, a more practical solution proves to be omitting the spike filter and fitting the spectra with adjustable base lines.

The reorientation of optically anisotropic scatterers appears as a broadening of the central component in the DDLS spectrum; the width is proportional to the rotation rate, and the intensity is proportional to the square of the polarizability anisotropy at optical frequencies. The rodlike and polarizable CPM molecules dominate the DDLS spectra recorded here. Figure 2 shows that the DDLS intensity recorded at the end of the experiment is proportional to CPM concentration, except for the two damaged samples. The 30% (w/w) CPM sample was burned by excessive laser power, and the 40% (w/w) CPM sample imploded at −4.5 °C because of its extreme adhesion and large thermal expansion coefficient. Rotational diffusion coefficients from the latter sample are not compiled here because of their poor precision. The blank indicated in Figure 2 is a dilute aqueous suspension of 91-nm-diameter polystyrene latex spheres that theoretically scatters no depolarized light but has a polarized scattering intensity comparable to that of the other samples.

Data analysis is performed by fitting the 400 points that comprise each DDLS spectrum to one or two Lorentzians plus a base line

$$I_{VH}(\omega) = \sum_{i=1}^{1 \text{ or } 2} N_i \frac{\Gamma_i}{\omega^2 + \Gamma_i^2} + \text{base line} \qquad (1)$$

The PMMA-containing samples' spectra are all fit to two Lorentzians: a narrow one whose width is similar to the instrumental line width, and a wider or "broadened" component that gives the CPM rotational rate.

Table I
Experimental Densities and Absolute Shear Viscosities of Neat CPM[a]

T, ±0.1 °C	ρ, g/mL	T, ±0.1 °C	η_s, cP
−4.5	1.137 493	−4.5	11.91
10	1.133 88	6.8	7.74
22	1.123 05	18.5	5.35
36	1.112 27	36	3.49
50	1.100 80	42	3.08
65	2.088 93	60	2.66
80	1.076 93	57	2.39
85	1.072 89	65	2.07
		73	1.86
		80	1.67
		89	1.45
		96.7	1.31

[a] Methanol density is measured as the standard, giving a 0.01% sample standard deviation.

The polarized spectra are analyzed for their Brillouin shift, which is proportional to the longitudinal adiabatic sound speed in the sample, c_s

$$\Delta\omega_B = qc_s = \frac{4\pi n}{\lambda} \sin\left(\frac{\phi}{2}\right) c_s$$

Here q is the magnitude of the scattering vector, n is the sample refractive index, λ is the illuminating wavelength in vacuo, and ϕ is the scattering angle, which is equal to 90° for all the DLS experiments reported here.

Values and confidence limits for the apparent rotational diffusion coefficients and the relative intensities of all rotational relaxations of CPM are compiled from three least-squares fits to each of at least three DDLS spectra at each FSR for each sample at each temperature. Since more than one FSR is employed experimentally at each temperature, it is possible to resolve more than one rotational rate in each sample when multiple relaxations exist; that is, the same sample studied at the same temperature often gives different rotational relaxation rates (widths of the "broadened" Lorentzian) when studied at different FSR's. In general, in such a situation, it might be expected that the best procedure would be to fit each spectrum at a given FSR with a sum of more than two Lorentzians (or a continuous distribution of Lorentzians). However, such fits are not unique, and the procedure described above of fitting each spectrum to, at most, a sum of two Lorentzians has been adopted. This procedure, as discussed in the Results, gives a set of discrete rotational relaxation rates for each sample at a given temperature, the different rates corresponding to the widths of the broadened Lorentzian measured at different FSR's. It is difficult to assess the quantitative validity of these relaxation times, although they are highly reproducible. The fastest of these rotational rates is probably the most significant and corresponds to the "fast time" studied by Ouano and Pecora.[4]

Results

Table I gives experimental density and absolute shear viscosity values of neat CPM for the −4 to +97 °C range. The density is linear in temperature within experimental error

$$\rho \text{ (g/mL)} = 1.3682 - 8.26 \times 10^{-4} T \text{ (K)} \qquad (\pm 0.05\%) \qquad (2)$$

Viscosity follows a form similar to the Vogel–Tamann–Fulcher (VTF) expression,[9] but with a nonzero intercept (Figure 3)

$$\eta_s \text{ (cP)} = 1.28 \exp\left[\frac{144}{T \text{ (K)} - 208}\right] - 1.8 \qquad (\pm 0.075\%) \qquad (3)$$

Fitting viscosity of neat CPM to the VTF equation gives rise to significant systematic deviations, as shown by the residuals plot in Figure 4.

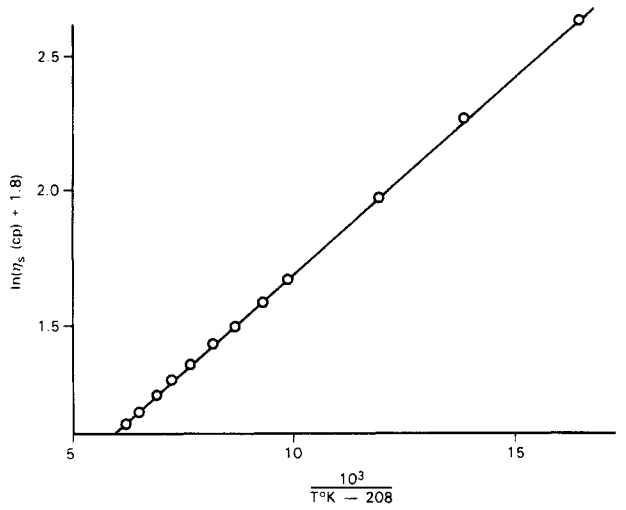

Figure 3. The modified VTF expression fits the viscosity temperature dependence in neat CPM to within the limits of experimental precision. Error bars representing ±1 sample standard deviation of the data are smaller than the data symbols below.

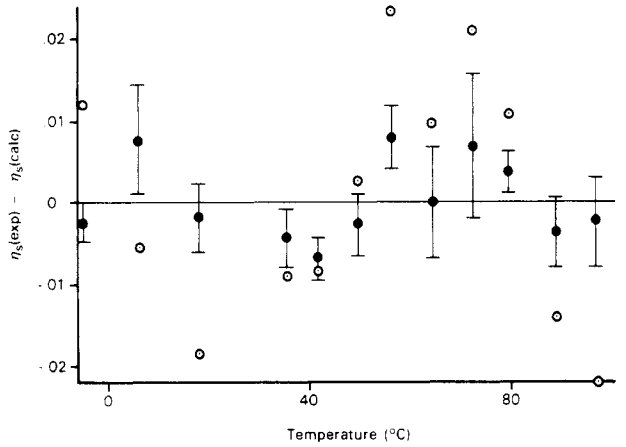

Figure 4. Residuals from two fits of the experimental viscosity of neat CPM to temperature-dependent expressions: $y = \eta_s$(exptl) $- \eta_s$(calcd), where ln η_s(calcd) (cP) = 546/T (K) − 152 − 2.2 (open circles) and ln (η_s(calcd) + 1.8) (cP) = 144/T (K) − 208 + 0.3 (filled circles). Error bars representing ±1 sample standard deviation of the data are only indicated on the filled circles for clarity.

Table II shows the longitudinal adiabatic sound speed in each sample as a function of temperature. The refractive index of each CPM/PMMA sample is calculated as the sum of the indices of each component weighted by its percent (by weight) in that sample. The index of neat CPM is measured with an Abbe refractometer and found to be n_D = 1.5856 at 22.2 °C. The PMMA refractive index is more difficult to measure, so an estimate for a well-annealed sample of 1.5 is assumed here. Figure 5 shows that the sound speed is inversely proportional to temperature within the considerable experimental error.

Table III presents the results of one- and two-Lorentzian fits to the DDLS interferometry spectra of CPM and CPM/PMMA solutions as a function of temperature. The results include the apparent rotational diffusion coefficient Θ derived from the half-width at half-maximum (HWHM) Γ_1 of the "broadened Lorentzian" that best fits the data and the dynamic/static intensity ratio K derived from the relative intensities of the broadened and narrow components of a two-Lorentzian fit (eq 1)

$$\Theta \equiv \tfrac{1}{6}\Gamma_1$$

$$K \equiv N_1/N_2 \qquad (4)$$

Table II
Brillouin Splitting and Longitudinal Adiabatic Sound Speed in CPM/PMMA with Selected Landau-Placzek Ratios

% (w/w) CPM	T, °C	$\Delta\omega_B$,[a] MHz	V_s, m/s	$I_{VV}(\delta(\omega))/2I_B$
20.34	−4.4	13136	2976	~120
	18.5	11102	2665	
	36	10937	2500	
	50	10909	2504	
	65	10238	2360	
	80	9816	2271	
	98	9149	2127	14
30.09	−4.4	12471	2802	~100
	18.5	10842	2587	
	36	10579	2408	
	50	10180	2328	
	65	9551	2194	
	80	9071	2094	
	98	8538	1983	12
49.15	−4.4	11432	2533	~50
	18.5	9509	2243	
	36	9073	2045	
	50	8623	1956	15
	65	7885	1800	
	80	7475	1718	
	98	6731	1559	7
57.68	−4.4	10463	2303	~20
	18.5	8599	2018	
	36	8259	1854	
	50	7916	1789	8
	65	7050	1605	
	80	6887	1580	
	98	6205	1436	4
100	−4.4	8457	1806	3
	18.5	7294	1578	
	36	6704	1482	
	50	6680	1484	
	65	6197	1392	
	80	5999	1363	
	98	5536	1275	3

[a] At 488 nm.

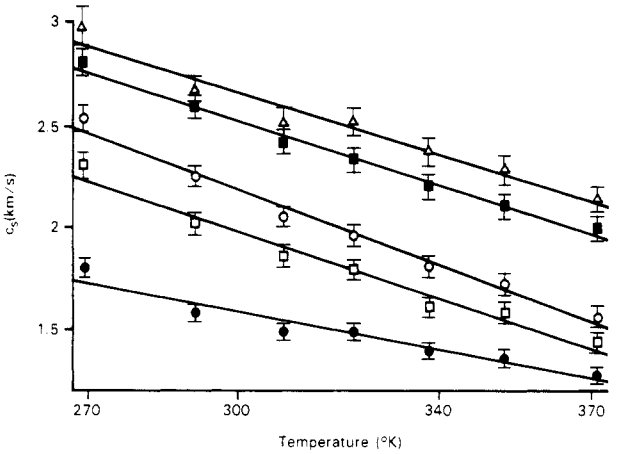

Figure 5. Longitudinal adiabatic sound speeds in CPM/PMMA samples. % (w/w) CPM: triangles, 20.3; filled squares, 30.1; open circles, 49.2; open squares, 57.7; filled circles, 100.

The intensities of the broadened and narrow Lorentzians from a fit to a spectrum are N_1 and N_2, respectively. The HWHM of the narrow Lorentzian Γ_2 cannot easily be transformed to a microscopic diffusion rate because it represents the convolution of instrumental parameters such as the mirror alignment with the spectral broadening due to the slow motion of the scatterers. The Γ_2 values of the fits to the CPM/PMMA samples' spectra grow steadily with increasing temperature, from the instrumental HWHM at −4.5 °C to nearly twice that value at 98 °C. However, numerical deconvolution to extract the

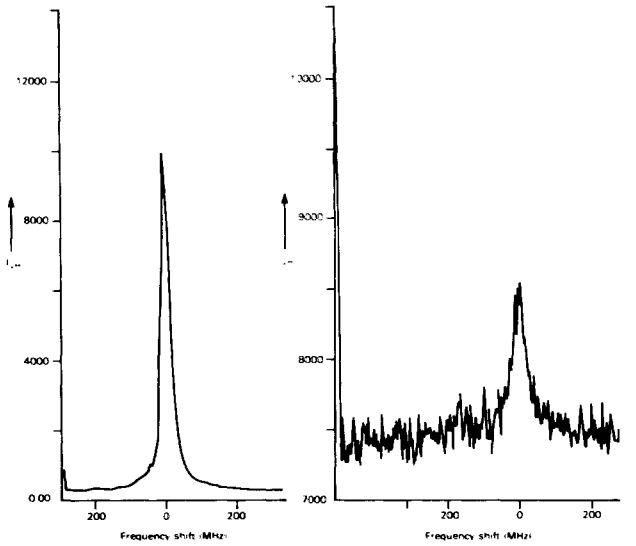

Figure 6. The central component intensity from DDLS spectra of CPM/PMMA samples is temperature dependent. Below are spectra recorded of 58% CPM at 0.75-GHz FSR. Note the vertical intensity scales. The spectrum at the left is taken at −4 °C and that at the right at +98 °C.

line widths of the narrow line is not performed here, so that Γ_2 values are not compiled. Figure 6 shows DDLS spectra of the 58% CPM sample at temperatures of −4 (left) and 98 °C recorded at 0.75-GHz FSR. Note the decrease in the intensity of the central portion ("unbroadened component") of the spectrum as the sample is heated. This decrease corresponds to an increase in K (see Table III).

The intensity ratio K in its simplest interpretation represents the number of CPM rods reorienting quickly divided by the number rotating slowly.[4] The limits on "fast" and "slow" are determined by the choice of experimental FSR; the fastest relaxation observable is no more than $^1/_3$ the FSR, while the slowest distinguishable relaxation is no less than $^1/_{30}$ the FSR. Several decades of spectral sensitivity are achieved by using multiple overlapping ranges, thereby ensuring that any CPM rotational relaxation of significant intensity within the 20-MHz to 100-GHz span is detected. If the rotational motions occurring simultaneously differ in rate by at least a factor of 3, they can be considered distinct processes. The K values of the different processes represent a dynamic/static intensity ratio, where the limits on "dynamic" and "static" are controlled by the choice of FSR. An overall K can be calculated that is the ratio of CPM molecules reorienting on interferometric time scales (≥20 MHz) to those (≤10 MHz) that are essentially static

$$K_0 = (1 - B - \delta)/\delta$$

Here B is the fraction of the depolarized scattered light appearing in the base line of the DDLS spectrum at a large FSR and δ is the fractional intensity in the central (narrow) component of the spectrum seen at the smallest (750 MHz) FSR. Any weak or very broad relaxation trends that could not otherwise be resolved are thereby included in the K_0 calculation, along with the principal relaxation pathways. The K_0 values are assembled in Table III.

The DDLS spectra of neat CPM show the well-known central dip[10] at all but the lowest temperature (Figure 7). This feature arises from the coupling of rotation of anisotropic molecules to hydrodynamic shear strain in the surrounding fluid. This central dip may be modeled as the sum of a positive wide and a negative narrow Lorentzian. Table III, thus, lists negative K values corresponding to this effect.

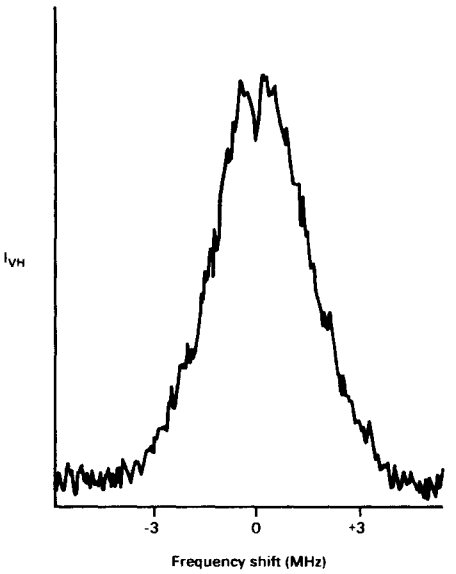

Figure 7. This room-temperature DDLS spectrum of neat CPM shows the central dip, which is observed throughout the 20–80 °C range.

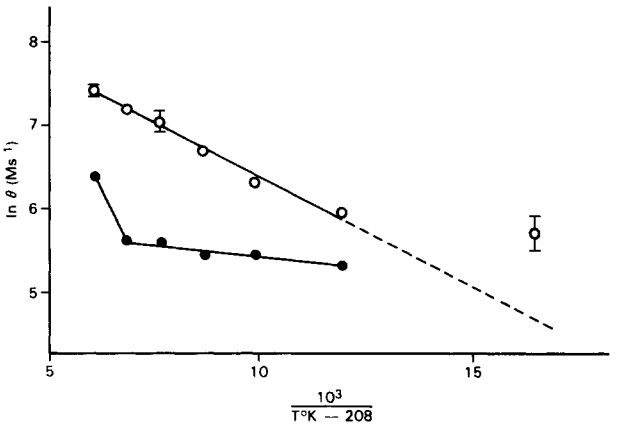

Figure 8. Neat CPM rotational diffusion coefficients are shown with error bars representing ±1 sample standard deviation (open circles). The HWHM of the central dip is given with no estimate of its relative error (filled circles).

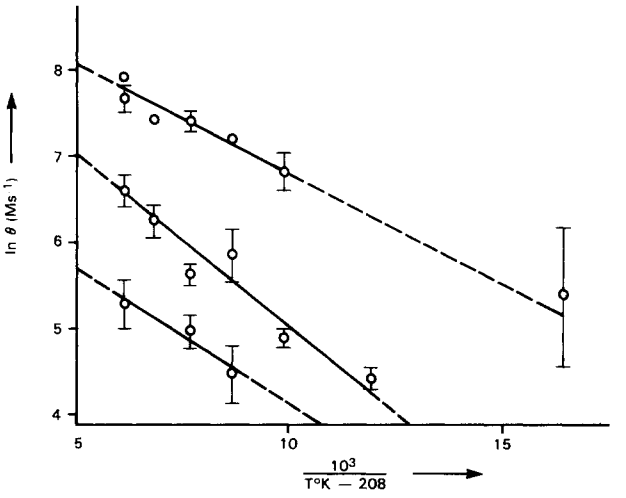

Figure 9. Multiple relaxation trends indicated by line segments are observed in DDLS spectra of 58% CPM in PMMA. Error bars are ±1 sample standard deviation of the data.

Discussion

Figures 8–11 show that the temperature dependences of the apparent rotational diffusion coefficients of CPM

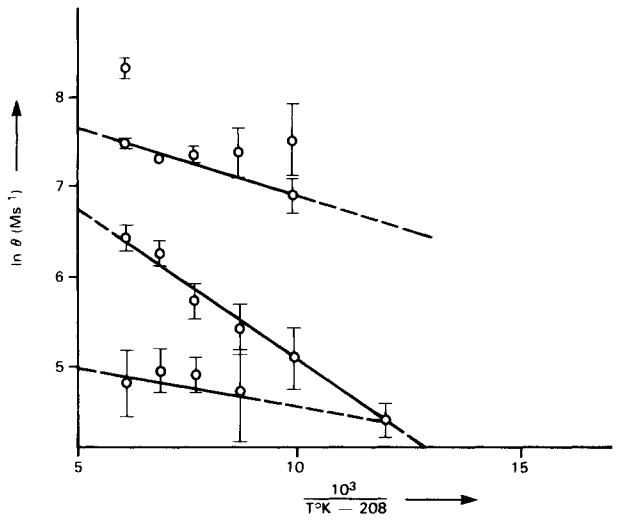

Figure 10. Multiple relaxation trends observed in DDLS spectra of 49% CPM in PMMA are indicated by line segments. Error bars are ±1 sample standard deviation. The fastest rate seen at 98 °C equals the rotational diffusion coefficient of neat CPM at the same temperature.

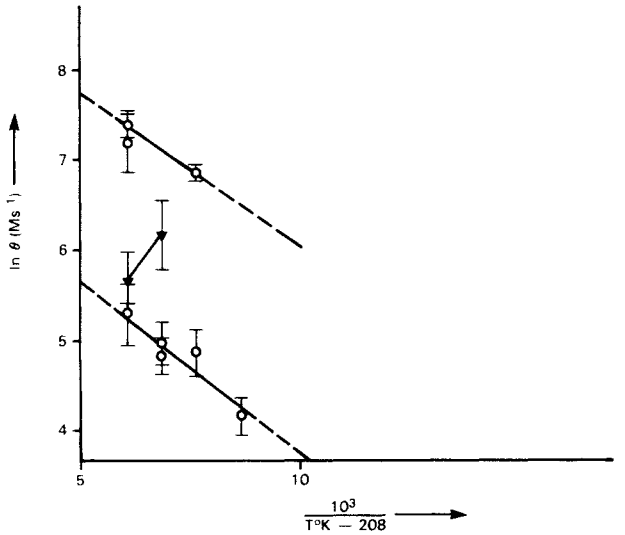

Figure 11. Multiple relaxation trends observed in DDLS spectra of 30% CPM in PMMA are shown with line segments (open circles). Only two data points are recorded from spectra of 20% CPM in PMMA (filled triangles). Error bars are ±1 sample standard deviation.

in the neat liquid and in PMMA mixtures fit well to the VTF form

$$\ln \Theta = a - b/[T\,(\mathrm{K}) - 208] \qquad (5)$$

In view of eq 3 and the predictions[11] of hydrodynamic models that $\eta_s \propto 1/\Theta$ + constant, this temperature dependence is not unexpected in the neat liquid CPM. The neat CPM data obey this proportionality at all but the −4.5 °C point (Figure 12). It is surprising, however, to see the same $1/(T - 208)$ dependence in the CPM rotation rates obeyed in CPM/PMMA samples, as indicated by line segments in Figures 9–11. These data are all derived from an averaged HWHM of the wider or "broadened" member of the two Lorentzians fit to the spectra of each sample at a given FSR, as discussed in the Experimental Section. All observed reorientation rates in CPM/PMMA samples are slower than that of neat CPM at the same temperature; the most intense and fastest relaxation rate approaches the rate seen in neat CPM in the limits of high temperature or CPM concentration, in agreement with the results of Ouano and Pecora.[4] The slowest relaxation trends

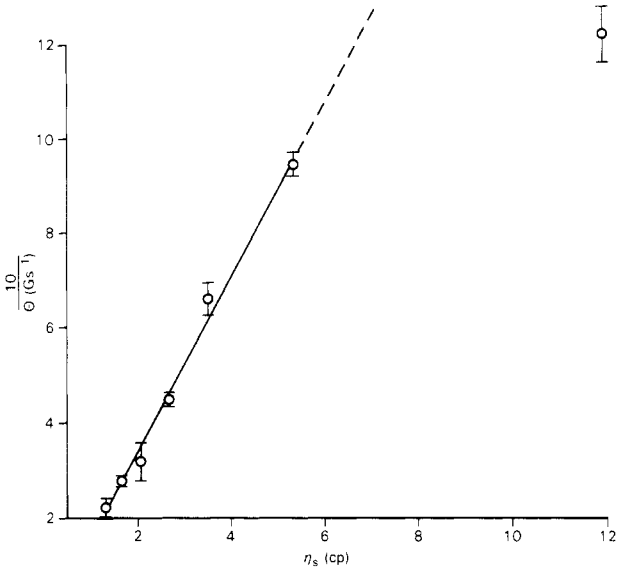

Figure 12. Rotational rates in neat CPM vary inversely with shear viscosity, except at the lowest temperature point. The error bars are the calculated standard deviations from DDLS spectral widths.

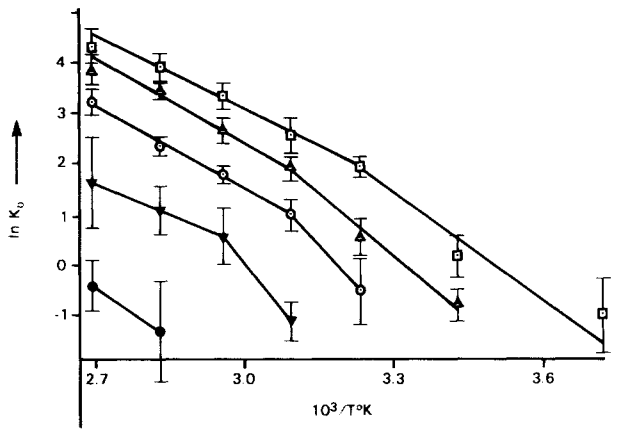

Figure 13. The arrhenius plots of the overall intensity ratios K_0 from CPM/PMMA spectra gives a concentration-independent apparent activation energy. Error bars are ±1 sample standard deviation. % (w/w) CPM: open squares, 57.7; open triangles, 49.2; open circles, 39.6; filled triangles, 30.1; filled circles, 20.3.

represent only ~2% of the depolarized spectral intensity and so have larger standard errors than the fast reorientation times. Note that the three relaxation trends depicted in Figure 9 and 10 and the two trends appearing in Figure 11 are clearly separated by at least a factor of 3 in rate. Note from Table III that often the same fast time (to within experimental error) is obtained for the same system observed at rather different FSR's. For example, the 49% CPM sample at 36 °C and 30% CPM sample at 98 °C both give the same fast component when it is observed at two different FSR's.

The intensities of each relaxation trend tend to increase with rising temperature. The fastest rotational relaxation trend observed becomes the principal relaxation pathway at high temperature or CPM concentration, representing perhaps $^3/_4$ of the depolarized scattered intensity. The most precise intensity data are the overall ratios K_0, which are shown in an Arrhenius plot in Figure 13. At high temperature, the apparent activation energy derived from the K_0 approaches a constant value of $\Delta E^{\ddagger} = 11.6 \pm 1.2$ kcal/mol for all the CPM/PMMA samples. The remaining K data are useful in interpreting the individual CPM/PMMA relaxation trends, with the restricted rota-

Table III
Apparent Rotational Diffusion Coefficients and Relative Intensities of CPM/PMMA Spectra

% (w/w) CPM	T, °C	Θ, Ms^{-1}	K	K_0	FSR, GHz
20.34	80	450 ± 142	0.26	0.26	0.75
	98	284 ± 68	0.65	0.65	0.75
30.09	50	62 ± 12	0.52	0.52	0.75
	65	126 ± 31	0.42	2.84	0.75
		919 ± 77	0.32		1.90
	80	141 ± 31	0.31	4.82	0.75
		120 ± 20	0.30		2.83
	98	194 ± 57	0.89	8.33	0.75
		1306 ± 387	0.72		2.94
		1556 ± 229	0.53		25.32
49.15	18.5	79 ± 14	0.44	0.44	0.75
	36	158 ± 45	0.77	1.69	0.75
		973 ± 169	1.64		2.94
		1790 ± 596	0.23		15.89
	50	110 ± 35	1.89	7.05	0.75
		218 ± 52	0.68		1.90
		1573 ± 379	0.34		19.65
	65	132 ± 24	1.82	14.34	0.75
		299 ± 53	2.38		1.90
		1556 ± 114	0.55		13.81
	80	138 ± 31	1.14	31.63	0.75
		513 ± 66	1.67		2.83
		1464 ± 69	1.64		22.06
	98	122 ± 36	1.54	46.67	0.75
		624 ± 83	1.45		2.94
		1775 ± 95	3.21		25.32
		4092 ± 437	0.62		50.88
57.68	-4.4	225 ± 124	0.37	0.37	0.75
	18.5	84 ± 10	1.18	1.18	0.75
	36	133 ± 13	1.72	6.82	0.75
		931 ± 185	0.51		2.94
	50	87.8 ± 25	1.44	12.83	0.75
		355 ± 91	1.92		1.90
		1368 ± 55	1.20		19.65
	65	147 ± 27	2.06	28.14	0.75
		283 ± 33	3.74		1.90
		1687 ± 176	1.60		13.81
	80	528 ± 85	2.86	48.81	2.83
		1716 ± 66	3.84		22.06
	98	200 ± 51	2.62	74.29	0.75
		758 ± 126	2.72		2.94
		2186 ± 303	5.84		25.32
		2824 ± 138	3.67		50.88

% (w/w) CPM	T, °C	Θ, Ms^{-1}	K^a	Γ_{dip}, Ms^{-1}
100	-4.4	822 ± 114		
	18.5	1058 ± 27	-4.17	3410
	36	1508 ± 78	-6.11	3962
	50	2214 ± 65	-21.29	3872
	65	3111 ± 346	-58.42	4366
	80	3579 ± 102	-13.19	4472
	98	4482 ± 340	-18.70	9853

[a] The ratios of intensities for the two Lorentzians that fit the spectral data are negative because the central "dip" is represented by a negative Lorentzian.

tional diffusion (RRD) theory.[6]

The Wang and Pecora RRD model assumes that the free rotational diffusion of a rodlike molecule in a hindering environment can only occur within some tubular region of space that constrains the rod's motion for a time that is long compared with the rod's unhindered rotational diffusion time. The angle through which free rotational diffusion can proceed is the "cone angle" θ_0, which ultimately affects both the effective rotational diffusion coefficient and the intensity of the relaxation observed in the DDLS spectrum. Restricting the rods' rotation causes some residual orientational correlation to persist, giving rise to an unbroadened component in the DDLS spectrum along with the dynamic (broadened) contribution. For ease of calculation, this RRD theory assumes that the surroundings of the hindered rods are completely immobile, and so the narrowest component in the predicted spectrum is proportional to the Dirac δ function (a spike) at zero frequency shift. The relative area of the broadened spectral contribution divided by that of the δ-function peak is just the dynamic/static intensity ratio K, defined earlier. Of course, in any real system, the continuous slow relaxation of the rods' surroundings and the instrumental limitations both impart a finite width to the "unbroadened" component, but the K value calculated remains unchanged.

The principal difficulty with interpretation of the CPM/PMMA spectra in terms of RRD theory is that the predicted spectral features are not in general well-defined Lorentzians but rather a superposition of components of similar width that cannot be fit uniquely.[6] At large cone angles ($\theta_0 \geq 150°$), the predicted spectrum approaches the single Lorentzian expected for unrestricted rotational diffusion of rodlike probes. At small cone angles ($\theta_0 \leq 45°$), the DDLS spectrum is predicted to be a single dynamic (broadened) Lorentzian plus the narrow central component. Moreover, the single broadened Lorentzian predicted to appear in small-cone-angle spectra is significantly different in width from the Lorentzian expected on the basis of hydrodynamics. The best experimental test of RRD theory therefore involves sample conditions of low temperature and low CPM concentration, which represents the small-cone-angle limit.

The RRD theory[6] presumes immobile surroundings for the restricted scatterers, and as a result the predicted apparent rotational rates at small cone angles are faster than one might expect from a real system. According to the theory, the true rotational diffusion coefficient of the rods is relatively unaffected by their surroundings, but the voume in which they are constrained to move is so small that the rods can diffuse to their limits in a shorter time. The apparent rotational rate that is observed by light scattering is then a function of the true rotational diffusion coefficient and the mean cone angle of the scatterers. The true (unrestricted) rotational diffusion coefficient Θ_{RRD} is derived from the apparent rotational diffusion rate Θ by means of an "attenuation coefficient" ν_1 that is calculated from the relative intensities of the two Lorentzian components of the DDLS spectrum[6]

$$\Gamma_{VH} = \nu_1{}^1(\nu_1{}^1 + 1)\Theta_{RRD} = 6\Theta$$

Thus, the application of RRD theory in the small-cone-angle limit involves measuring a cone angle from the intensity ratio of the broadened to central DDLS spectral components, K, and deriving from it the attenuation coefficient ν_1 that relates the observed width of the broadened Lorentzian to the diffusion coefficient expected from unrestricted rotational diffusion at the same rate. Table IV is a compilation of attenuation coefficients, cone angles, and resulting Θ_{RRD} values for the relaxation trends in the DDLS spectra of the CPM/PMMA samples. If we momentarily ignore the slower trends, a comparison can be made to the results of Ouano and Pecora[4] for chlorobenzene (CB) in PMMA.

Figure 14 shows the cone angles derived from DDLS spectra of CB/PMMA and CPM/PMMA samples at comparable free spectral ranges: 13–50 GHz. The cone angles found for the two systems converge at ~100 °C but have different temperature dependences

$$\theta_0 = AT + B(c)$$

where

$$A = 0.15\ (K^{-1}) \pm 0.05 \text{ for CB}$$

$$A = 0.55\ (K^{-1}) \pm 0.05 \text{ for CPM}$$

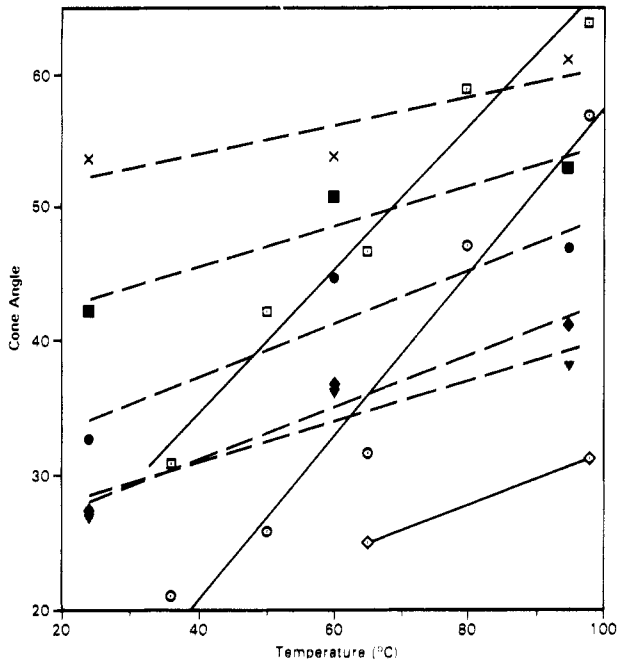

Figure 14. Cone-angle predictions from the fast relaxation intensity to CPM/PMMA spectra (solid lines) have a greater temperature dependence than cone angles calculated from CB/PMMA spectra (dashed lines). % (w/w) CPM: open squares, 57.7; open circles, 49.2; open diamonds, 30.1. % (w/w) CB: crosses, 60; filled squares, 50; filled circles, 40; filled diamonds, 28; filled triangles, 20.

The parameter $B(c)$ depends only on the solvent concentration. The much larger temperature dependence of the cone angle for the system of longer rods is consistent with the intuition that a longer probe is damped from rotating by its environment more than a shorter one. Less obvious is the fact that solvent concentration dependence of the cone angle becomes more pronounced as the temperature falls. As a result, the samples containing low CPM concentrations show no fast relaxation components at low temperatures and so cannot be compared to similar CB/PMMA samples.

In the hydrodynamic limit, where viscosity and rotational rate are inversely proportional, the concentration dependence of the DDLS spectral widths of the CPM/PMMA samples may be fit with Doolittle's empirical expression.[7] For concentrated high-polymer solutions, the VTF expression is approximated as

$$\ln \eta_s(c,T) = A + \frac{\exp[-kc^{-1/4}]}{T - T_0}$$

where c is the weight fraction of the solute, PMMA. In the limits of low temperature or CPM concentration, the fast relaxation rate is consistent with the predicted form

$$\ln \Theta(c) = \ln \Theta_{CPM} - a \exp[-kc^{-1/4}]$$

with $k \approx 20$. The slow relaxation trends observed and the transformed rotational diffusion coefficients do not exhibit any concentration dependence.

As explained previously the quantitative significance of the slower times is not clear. The precise numerical values obtained could very well be an artifact of the fitting procedure. What is clear from the data is that there are relaxation times in the approximate times ranges given. The presence of such times could be explained by incorporating relaxation of the cone walls. For instance, McCall has given a summary of NMR relaxation rate data for PMMA chain methyl reorientation.[12] This motion is effected by trans/gauche isomerization of the polymer backbone. The NMR data discussed by McCall are comparable in apparent activation energy ($\Delta E^{\ddagger} \sim 5$ kcal/mol) to those of the DDLS spectral slow components. Direct comparison of the relaxation rates is difficult, however, since the NMR experiments were performed at much lower temperatures than the light scattering experiments. If the linear trend in plots of the logarithms of the NMR correlation frequencies (ν_c) vs. $1/T$ is extrapolated toward higher temperatures by 40–120 °C, the NMR relaxation frequencies attributed to chain methyl reorientation are found to be similar to the averaged slow DDLS spectral HWHM values:

T, °C	18.5	36	50	65	80	98
extrap ν_c, MHz	69	121	182	170	390	580
slow Γ_{VH}, MHz	77	139	208	278	467	660

Although this correlation between these values could be a coincidence, it is more likely that they are, in fact, related: the chain methyl reorientation causes a relaxation of the local environment of the CPM that gives a DDLS relaxation time of the same order of magnitude.

Table IV
Cone Angles, Attenuation Coefficients, and Transformed Rotational Diffusion Coefficients Derived from Application of RRD Theory in the Small-Cone-Angle Limit

% (w/w) CPM	T, °C	K	θ_0^0	$\nu_1^1(\nu_1^1 + 1)$	Θ_{RRD}, Ms^{-1}
20.34	80	0.26	23	22.6	115
	98	0.65	32.5	11.2	152
30.09	50	0.52	31	12.2	30.5
	65	0.42	28	15.1	50.0
		0.32	25	18.8	293
	80	0.31	25	18.8	44.8
		0.30	24.5	19.6	36.7
	98	0.89	38	8.3	140
		0.72	35	9.8	800
		0.53	31.5	11.9	785
49.15	18.5	0.44	29	14.0	33.9
	36	0.77	36	9.2	103
		1.64	47	5.6	1042
		0.23	21.5	25.7	418
	50	1.89	49.5	5.3	65.4
		0.68	34.5	10.1	130
		0.34	26	17.3	546
	65	1.82	49	5.3	149
		2.38	52.5	4.8	374
		0.55	32	11.5	812
	80	1.14	42	6.8	124
		1.67	47.5	5.6	550
		1.64	47	5.6	1569
49.15	98	1.54	46	5.8	126
		1.45	45	6.0	624
		3.21	57	4.1	2598
		0.62	33	11.0	2232
57.68	-4.4	0.37	27	16.2	83.3
	18.5	1.18	42	6.8	75.2
	36	1.72	48	5.5	145
		0.51	31	12.2	458
	50	1.44	45	6.0	87.8
		1.92	50	5.2	410
		1.20	42	6.8	1207
	65	2.06	50.5	5.1	173
		3.74	58	3.9	435
		1.60	47	5.6	1808
	80	2.86	55	4.4	720
		3.84	59	3.8	2709
	98	2.62	53.5	4.6	261
		2.72	54	4.5	1011
		5.84	64	3.2	4099
		3.67	58	3.9	4345

Conclusion

Several modes of rotational relaxation of CPM in PMMA are observed by interferometry that have apparent

activation energies of 1–11 kcal/mol and widely separated speeds. The RRD theory qualitatively explains these DDLS spectral results. In terms of the theory, the orientational correlation function measured in DDLS spectra of CPM/PMMA samples initially decays at a rapid rate characteristic of neat CPM, indicating a restricting cone angle of about 25–60°. The RRD theory predicts from the intensity and rate of this initial decay a "true" or transformed rotational diffusion coefficient that is not very different from that of neat CPM (and approaches it at high concentrations and temperatures). After the rapid initial decay, the orientational correlation function then decays over a wide range of time scales that apparently reflect the slower relaxation rates of the restricting surroundings. The simple RRD theory used here does not quantitatively treat coupling between the rods and their restricting environment so that it cannot predict the form of the orientational correlation function over the entire relaxation range. Extensions of the RRD theory to include these couplings would be very useful in interpreting the slower relaxation times observed in these experiments.

Acknowledgment. This work was supported by National Science Foundation Grant No. CHE 82-00512, the IBM Corp., and the NSF–MRL program through the Center for Materials Research at Stanford University.

Registry No. CPM, 831-81-2; PMMA, 9011-14-7.

References and Notes

(1) Higashigaki, Y.; Wang, C. H. *J. Chem. Phys.* **1981**, *74*, 3175.
(2) Patterson, G. D. *Annu. Rev. Mater. Sci.* **1983**, *13*, 219.
(3) Dorfmüller, T., et al. *J. Chem. Phys.* **1979**, *71*, 366.
(4) Ouano, A. C.; Pecora, R. *Macromolecules* **1980**, *13*, 1167, 1173.
(5) Berne, B. J.; Pecora, R. "Dynamic Light Scattering"; Wiley: New York, 1976.
(6) Wang, C.-C.; Pecora, R. *J. Chem. Phys.* **1980**, *72*, 5333.
(7) Doolittle, A. K. *J. Appl. Phys.* **1952**, *23*, 418.
(8) "International Critical Tables of Numerical Data, Physics, Chemistry and Technology"; McGraw-Hill, New York: Vol. 3, pp 27, 28; Vol. 5, p 26; Vol. 7, p 213.
(9) Bohdaneckŷ, M.; Kovâř, J. "Viscosity of Polymer Solutions"; Elsevier Scientific: New York, 1982; pp 202, 208.
(10) Berne, B. J.; Pecora, R., ref 5, pp 143–150.
(11) Bauer, D. R.; Brauman, J. I.; Pecora, R. *Annu. Rev. Phys. Chem.* **1976**, *27*, 443.
(12) McCall, D. W. *Acc. Chem. Res.* **1971**, *4*, 223.

Normal-Coordinate Analysis of the Dynamics of Cubic Lattice Models of Polymer Chains

Michelle Dial, Katherine S. Crabb,† Charles C. Crabb,† and Jeffrey Kovac*

Department of Chemistry, University of Tennessee, Knoxville, Tennessee 37996-1600.
Received March 4, 1985

ABSTRACT: The dynamic behavior of isolated cubic lattice model polymer chains was simulated with and without excluded volume by using a Monte Carlo method. The chain relaxation was analyzed by using the Rouse normal coordinates. For the first three normal modes we find that the relaxation times conform fairly well to the prediction of the Rouse theory in the absence of excluded volume, but in the presence of excluded volume, there are deviations in both the N dependence and the k dependence of the relaxation times.

Introduction

In a recent paper Gurler, Crabb, Dahlin, and Kovac[1] developed a model for the simulation of the dynamics of cubic lattice models of polymer chains using a Monte Carlo method. This model differed from most of the previous work[2] on the cubic lattice model in that one of the elementary motions employed was the 90° crankshaft. The dynamics of isolated chains were studied both in the presence and absence of excluded volume. Both the end-to-end vector relaxation time and the center-of-mass diffusion constant were computed, and the results were found to agree fairly well with the results of the Rouse model[3] in the absence of excluded volume and with the scaling prediction for chains with excluded volume.[4] The model has been extended to multiple chain systems by Crabb and Kovac[5] in order to investigate the effects of entanglements on chain dynamics.

The results of Gurler, Crabb, Dahlin, and Kovac raised several questions that prompted the more detailed study of the chain dynamics reported in this paper. The first question concerns the calculation of the end-to-end vector relaxation time, τ_R. In the paper of Gurler, Crabb, Dahlin, and Kovac this quantity was estimated by first computing the end-to-end vector autocorrelation function, $\rho_R(t)$, defined by

$$\rho_R(t) = \frac{\langle \vec{R}(t)\cdot\vec{R}(0)\rangle}{\langle \mathbf{R}^2\rangle} \quad (1)$$

where $\langle\ \rangle$ denotes an equilibrium ensemble average. This average was computed as a time average. A least-squares line was then fit to the linear, long-time region of a semilog plot of $\rho_R(t)$ vs. t. The negative of the relaxation time, τ_R, is then the inverse of the slope of this line. There is an obvious problem with this calculation. A choice of the linear region to be fit must be made, and this choice is somewhat arbitrary. Gurler, Crabb, Dahlin, and Kovac took care not to introduce bias through the choice of the linear region, but questions concerning the accuracy of their relaxation times remain. A less controversial procedure would be to calculate the autocorrelation function of the first ($k = 1$) normal coordinate and calculate the relaxation time from the slope of a semilog plot of that function vs. time. The normal coordinates, $\tilde{U}_k(t)$, are defined by[6]

$$\tilde{U}_k(t) = \sum_{j=1}^{N} \left(\frac{2-\delta_{k0}}{N}\right)^{1/2} \cos\left[(j-1)\pi k/N\right]\vec{R}_j(t) \quad (2)$$

where $\vec{R}_j$ is the position of the jth bead with respect to the origin. The autocorrelation function of the kth normal coordinate, $\rho_k(t)$, is given by

* To whom correspondence should be addressed.
† Present address: Rohm and Haas Research Laboratories, Rohm and Haas Company, Bristol, PA 19007.

0024-9297/85/2218-2215$01.50/0